An Optical Proximity Sensor for Measuring Surface Position and Orientation for Robot Manipulation

Takeo Kanade and Thomas M. Sommer

CMU-RI-TR-83-15

Robotics Institute
Carnegie-Mellon University
Pittsburgh, Pennsylvania 15213

September 5, 1983

This research was supported by the Robotics Institute, Carnegie-Mellon University, and in part, by the Office of Naval Research.

Abstract

We have developed a noncontact proximity sensor which can measure the distance and orientation of a surface in a range of four to five centimeters. The sensor is based on the scheme of active illumination and triangulation. It uses multiple infrared LEDs as the light sources and a PIN-diode area sensor chip for detecting the spot positions. Six LEDs with optics for collimating the beam are mounted at the sensor head. The directions of the beams are aligned to form a cone of light converging at a distance of 4.5 cm from the sensor head. As each LED is sequentially pulsed, the sensor chip detects the position, in its field of view, of the spot projected by the LED light beam on the object surface. The 3-D location of the spot on the surface can be computed by triangulation. By doing this for six LEDs we obtain a set of six 3-D points. Then by fitting a plane to those points, the distance and orientation of a small portion of the object surface are calculated.

Since there is no moving part and the spot position sensor chip is an analog sensor which outputs the position of the spot directly without scanning its field of view, we can realize fast operation of our proximity sensor. Currently the sensor can give approximately 1000 measurements of distance and orientation per second with precision of 0.07 mm for distance and 1.5^{o} for surface orientation. This non-contact proximity sensor will be useful for such applications as tracing an object surface by a robot arm with specified distance and orientation relative to the surface.

1. Introduction

Recently considerable effort has gone into research on rangefinding sensors. The quantity to be measured in range finding includes distance, surface orientation, surface curvature, and additional surface properties such as reflectivity. Proximity sensors grew from the need to gain environmental information in close proximity to the robotic device. They occupy a unique niche in the range of sensors in that it bridges the sensing gap between the gross imaging of vision systems and the direct contact of tactile sensors. The spatial measurement capability of the proximity sensor allows a representation to be constructed of the local environment.

Many types of proximity sensors have been built. The simplest sensors are proximity switches capable of merely detecting the presence or absence of an object in the sensor's proximity. More complex proximity sensors have the capability of determining continuous three-dimensional position and other information such as intensity and orientation. Different proximity sensors employ various media including magnetic field, electric field, air pressure, ultrasonic sound, and light. Recent advance in inexpensive electro-optical components also has made optical methods attractive.

Simple optical proximity sensors can be built based on the sensitive-volume technique [1]. The intersection of a cone of emitted light and the field of view of the detector forms a roughly cigar-shaped sensitive volume in space. When an object enters this sensitive volume, light is reflected and strikes the detector, which generates a voltage corresponding to the depth. One problem of this technique is that the detector output tends to show a bell shaped curve as a function of the depth, and therefore two different depths can give the same output which can lead to confusion. This problem can be solved by recessing the detector inward so that only the outer portion of the range curve is used. A more serious problem is that the measurement is affected by surface reflectivity and surface orientation.

To overcome some of the limitations of the sensitive-volume approach, Okada recently developed a proximity sensor with multiple sources and a single detector [3]. It employs a photo transistor and multiple miniature incandescent lamps which are linearly placed. The light sources are sequentially lit, and the emitted light is projected on the object surface through a pin hole. The diffusely reflected light is received by the photo transistor through another pin hole. Therefore an individual pair of a light source and the receiver forms a sensitive-volume sensor. Okada has shown that even though the bell shaped curve of the receiver output itself is sensitive to surface orientation and reflectance, the distance at which the output takes its peak is very stable. Thus, the distance measurement is based on the number of the light source for which the output becomes maximum with appropriate interpolation to obtain continuous measurement in between. This sensor exploits the geometrical arrangement to increase reliability.

The proximity sensor we have developed differs from these optical proximity sensors in that it employs multiple infrared LEDs as the light sources and a PIN-diode area sensor chip for detecting the spot positions, and that it is based on triangulation. It can gather information of multiple spatial point locations on a local surface patch, and therefore can also compute the surface orientation. The features of this sensor include simplicity, high-speed operation, versatility, and accuracy due to the redundancy in its geometry. This paper presents the theory, implementation, and performance of our proximity sensor.

2. Design of the Proximity Sensor

2.1. Overview

Figure 1 is a photo of the prototype of the proximity sensor we have built. The configuration of the proximity sensor is shown in Figure 2. The sensor head consists of multiple light sources (six LEDs in the case of the prototype we have built), an objective lens, and a sensor chip acting as a spot-position detector. The sensor is controlled by an LSI 11 microprocessor. The six light sources are placed in a circular pattern 60° apart pointing towards the optical axis of the objective lens. Light sources are aligned so that all six light source beams cross the optical axis at the same point. The light beams thus form an optical cone. The tip of the cone is placed at approximately the center of the range of operation of the proximity sensor. Each light source is independently controllable.

The objective lens and sensor chip form a camera arrangement. When an object intercepts the light beam, the resultant light spot is imaged onto the sensor chip through the objective lens. The sensor chip then gives the spot position on its active two-dimensional face. Knowledge of the spot position on the sensor chip (together with the camera optics) and the trajectory of the light beam allow us to perform triangulation and to find the coordinates of the point in three-dimensional space. From the measurement of multiple points in the vicinity we can calculate information such as the surface orientation.

2.2. Geometry

Figure 3 shows the geometry of the device involving the light sources, the lens, and the sensor chip [2]. The x-y-z coordinate system is taken so that the origin is at the lens center, the z axis is along the optical axis. The light source LEDs are placed on the x-y plane and their coordinates are in general $(x_s, y_s, 0)$. Their rays point to $(0, 0, d)$ on the z-axis. and make the angle θ with the z axis. Suppose that the optical system is designed so that the plane $z = d$ through the converging point is at the best focus and that the plane is imaged on the sensor chip with a magnification factor M. To model this imaging geometry we can imagine the sensor chip is at $z = -Md$. In this case, a spatial point (x, y, z) is imaged on the sensor chip at $(x_c, y_c, -Md)$, where

$$x_c = -\frac{xMd}{z}$$

$$y_c = -\frac{yMd}{z}. \tag{1}$$

Let us take an LED on the x axis; ie, at $(x_s, 0, 0)$, and imagine a spot at $(x, 0, z)$ projected onto a surface. Since the spot is on the light beam,

$$z = (d\tan\theta - x)\cot\theta \tag{2}$$

The spot generates its image on the sensor at $(x_c, 0, -Md)$. From (1) and (2) we obtain the depth (z) as a function of the spot image location (x_c).

$$z = \frac{d}{1 - x_c/(dM\tan\theta)} \tag{3}$$

We can evaluate how sensitive this measurement of the depth is by calculating the amount of change in the image position x_c due to a change in the depth z.

$$S = \left|\frac{\Delta x_c}{\Delta z}\right| = \frac{d^2 M\tan\theta}{z^2} \tag{4}$$

The larger the S is, the more sensitive the measurement. Naturally, as (4) shows, the larger magnification and the more slanted beam give a greater sensitivity.

Another system parameter is the range of depth measurement. Assuming the effective chip size is L, this can be evaluated by the depths z_1 and z_2, at which the corresponding spot images are at the edge of the effective sensor field, i.e. $x_c = L/2$ and $x_c = -L/2$. The maximum measurable range W is therefore given as,

$$W = z_2 - z_1 = \frac{L/(M\tan\theta)}{1 - [L/(2dM\tan\theta)]^2} \tag{5}$$

Usually, in designing this device, the depth of interest d is given. The magnification factor M and the beam angle θ are design variables whose values have to be determined. The trade-off in determining M and θ is between the measurable range of depth W and the sensitivity S. The larger M and θ we choose, we have the larger S but smaller W, and vice versa. Practically, however, W can not be too large, because it has to be within a range of reasonable focus and distortion due to lens. The angle θ also should not be too large, because, if so, the amount of return light tends to be very small.

Having derived the relationships among the system parameters, we have chosen the following values for the prototype we have developed:

Depth of interest	$d = 45$ mm
Size of the sensor chip	$L = 11$ mm
Magnification	$M = 1$
Focal legth of object lens	$f = 22.5$ mm
Range of depth	$W = 11.2$ mm with $z_1 = 40.1$ mm and $z_2 = 51.3$mm
Sensitivity	$S = 1.14$ (at z_1) and .89 (at z_2)

2.3. Light Source

Each light source is comprised of a high power infrared light emitting diode (LED), an aperture, and a converging lens as shown in Figure 4. This configuration was chosen due to its small size, acceptable intensity, and small divergence of the beam. The light source is designed so that the smallest spot diameter is realized in the operational range of the proximity sensor.

The LED used is a Litronix SFH 400-3. It is a narrow beam ($\pm 6^{o}$ at the half power point) infrared emitter with 950 *nm* peak emission wavelength. The LED is over-driven for a short period of time and the estimated output power is 1.5 mW. The focal length of the collimating lens is 26mm, and together with an aperture of diameter 1.4 mm we obtain a spot of diameter about 2 mm in the operating range. An elliptical spot is created when the light beam is projected onto a slanted surface. As will be mentioned, the elliptical shape and the finite size of the light spot do not become a serious problem because of the ability of the sensor chip to find the intensity center.

2.4. Spot Position Sensing

The camera configuration for detecting the spot position is comprised of a two dimensional spot-position detector chip and a double convex objective lens. The camera is covered by nonreflective material to reduce unwanted reflections. The sensor chip is Hamamatsu S1300, which consists of a planar PIN photodiode with homogeneous resistive sheets on both sides. Figure 5 shows a simplified functional diagram of the sensor chip. The sensor chip has four outer electrodes (x_1, x_2, y_1, y_2). When a spot of light strikes the sensor chip face, a photocurrent source, I_0, is generated at the point. Consider a spot of light impinging on the sensor chip face at a point (x_c, y_c) where $-L/2 \le x_c, y_c \le L/2$ When the four electrodes of the sensor chip are terminated by identical resistors, R_0, the currents which appear at the electrodes are given by:

$$
\begin{aligned}
I_{x1} &= \frac{r(x_c + L/2) + R_0}{rL + 2R_0} I_0 \\
I_{x2} &= \frac{r(L/2 - x_c) + R_0}{rL + 2R_0} I_0 \\
I_{y1} &= \frac{r(y_c + L/2) + R_0}{rL + 2R_0} I_0 \\
I_{y2} &= \frac{r(L/2 - y_c) + R_0}{rL + 2R_0} I_0
\end{aligned}
\qquad (6)
$$

assuming that the unit resistance of the resistive sheets is $r\,\Omega$/mm. By evaluating the following quantities, X_c and Y_c, we obtain

$$X_c = \frac{I_{x1} - I_{x2}}{I_{x1} + I_{x2}} = \frac{2rx_c}{rL + 2R_0}$$
$$Y_c = \frac{I_{y1} - I_{y2}}{I_{y1} + I_{y2}} = \frac{2ry_c}{rL + 2R_0} \qquad (7)$$
$$I_0 = I_{x1} + I_{x2} = I_{y1} + I_{y2}$$

Therefore, values of X_c and Y_c give the position of the spot (x_c, y_c) on the sensor chip. The amount of the current source, I_0, is proportional to the intensity of the spot impinging on the face of the sensor chip. We can see that the sensor chip intrinsically finds the intensity-weighted center of light distribution. This feature is useful because the spot position detection tends to be insensitive to defocus or deformation of the spot.

The sensor chip requires a minimum light power of approximately 2 microwatts to operate. Only a small portion of the light reflected at the surface reaches the sensor chip. We can estimate the power reaching the sensor chip for a high diffuse reflective surface which is perpendicular to the optical axis as

$$P_{sc} = \frac{A^2 P_s}{4l^2}$$

where A denotes the diameter of the aperture of the objective lens, l, the path length along the optical axis, and P_s, the light source power. In our prototype sensor, A = 10 mm, and P_s = 1.5 mW. When the surface is at the center of the measurement range, ie, l = 45 mm, P_{sc} can be estimated as large as 15μW, which is more than adequate for operating the sensor chip. Using the responsivity .5A/W from the sensor chip data sheet we expect the output current I_0 = 15μW × .5A/W = 7.5μA.

Actually the load resistor R_0 is the input resistance of a current-to-voltage converter shown in Figure 6. The value of the feedback resistance R_b determines the conversion factor V_{out}/I_{in}, and the equivalent input resistance of the circuit (load resistance to the chip) is given by $R_0 = R_b/G$, where G is the open loop gain of the operational amp. Notice from equation (7) that R_0 should be small enough compared to the resistance of the chip for accurate measurement. Also, a smaller R_0 gives a faster response time. The value of R_b was set 330 KΩ. With an amplifier of gain 10^5, the input impedance (R_0) of our current to voltage converter is therefore,

$$R_0 = \frac{R_b}{G} = \frac{330K\Omega}{10^5} = 3.3\,\Omega$$

which is far smaller than the chip resistance rL = 15 KΩ.

2.5. Timing

The data acquisition proceeds in the following order: The LSI 11 sends a signal to turn on one of the LEDs. The spot position sensor responds to the light reflected at the object surface. When the output of the sensor circuit becomes stable, the four signals corresponding to I_{x1}, I_{x2}, I_{y1}, and I_{y2} go through sample-and-hold and digitization. Including the software latency at the LSI 11, the data acquisition is done within 166 μsec, which translates to a maximum acquisition rate of 6000 points/second.

3. Calculating Surface Location and Orientation

Calculation of the spatial location and orientation of the object surface consists of three steps: triangulation, error correction, and plane fitting. The calculation of triangulation and error correction is repeated for each of the light sources, and plane fitting is done after a set of six measurements is obtained.

3.1. Triangulation

Once we obtain the four values of I_{x1}, I_{x2}, I_{y1}, and I_{y2}, we can obtain the chip spot position (x_c, y_c) by using the equations (7). Then, we can determine the spatial coordinates of the spot by triangulation. The line trajectory of the light beam is constant for each LED, and the line of sight of the spot (line trajectory of the diffusely reflected light projected onto the sensor chip) is obtained from the chip spot position.

As shown in Figure 7 the line of light beam is defined by the light source origin $\vec{p_s}$ and the light beam direction vector $\vec{a_s}$,

$$\vec{p_s} = (x_s, y_s, 0),$$

$$\vec{a_s} = (a_s, b_s, c_s).$$

The line of sight is defined by the lens center and the direction of projection:

$$p_c = (0, 0, 0)$$

$$\vec{a_c} = (x_c, y_c, -Md)$$

Let us denote the coordinate of the spot position we want to locate as

$$\vec{p} = (x, y, z).$$

In theory, the two three-dimensional lines (the light source beam and the line of sight) should intersect and give the location of the spot on the surface. In reality, however, the two spatial lines thus obtained only come very close due to noise and the simplified optical model being used. We therefore determine the spot location $\vec{p}$ on the line of the minimum distance (ie, along the common normal) between the two lines. The direction of the common normal is $\vec{a} = \vec{a_s} \times \vec{a_c}$. By noticing that $\vec{p}$ is on the common normal, we obtain the following

equations:

$$(\vec{p}-\vec{p}_s)\cdot(\vec{a}_s\times\vec{a})=0$$

$$(\vec{p}-\vec{p}_c)\cdot(\vec{a}_c\times\vec{a})=0 \tag{8}$$

$$(\vec{p}-\vec{p}_c)\cdot\vec{a}=\lambda(\vec{p}_s-\vec{p}_c)\cdot\vec{a}$$

$$0\le\lambda\le 1.$$

λ is a factor to determine where $\vec{p}$ is placed along $\vec{a}$ depending on which of the two spatial lines are more reliable. In our sensor we have chosen λ to be 0.5, that is, $\vec{p}$ is half way between the line of the light source beam and the line of sight. By solving the above simultaneous linear equations we obtain the spatial location of a spot on the surface for each LED.

3.2. Error Correction

The optical model so far used has a few simplifications: first, the light source beam is a line and thus the projected light spot is a point; second, the camera optics has no distortion or defocus; and finally the sensor chip is linear in finding the chip spot position. Since various distortion and nonlinearity exist in reality, the spatial location $\vec{p}=(x,y,z)$ of the spot calculated by triangulation above based on this simplified model includes errors. Suppose that $(\bar{x}, \bar{y}, \bar{z})$ is the correct location, and let us put

$$\bar{x} = x + \varepsilon_x$$
$$\bar{y} = y + \varepsilon_y$$
$$\bar{z} = z + \varepsilon_z.$$

It would be very difficult to model the effect of the departures from the simplified model precisely to determine the terms ε_x, ε_y, and ε_z. However, since the errors are repeatable with respect to the measured chip position (x_c, y_c), we can model them as a whole by means of polynomials. Error correction polynomials of different orders were experimentally tested. It was found that third-order error correction polynomials gave the best result without prohibitively large computation. Thus we use

$$\varepsilon_t = f_t(x_c,y_c) = a_{t1}x_c^3 + a_{t2}x_c^2y_c + a_{t3}x_cy_c^2 + a_{t4}y_c^3 + a_{t5}x_c^2 + a_{t6}x_cy_c \tag{9}$$
$$+ a_{t7}y_c^2 + a_{t8}x_c + a_{t9}y_c + a_{t10}$$

where $t = x, y, z$.

In the phase of calibration before the actual operation of the proximity sensor, these polynomials are designed for each LED using a calibrated data set. In the phase of operation, the values ε_x, ε_y, and ε_z computed by equations (9) are added to the spatial coordinates (x, y, z) computed by triangulation to obtain the corrected location of the spot.

3.3. Plane Fitting

When we have obtained the spatial coordinates of a spot on the surface for each of six LEDs, we fit a plane to this set of six points by a least-square method and obtain the equation of a three-dimensional plane which represents the local surface patch:

$$ax + by + cz + d = 0 \tag{10}$$

where $\vec{n} = (a, b, c)$ is a normalized surface normal.

As shown in Figure 8, the location of the surface is measured by the distance from the origin to the point where this plane intersects the optical (z) axis:

$$D = \frac{-d}{c} \tag{11}$$

The surface orientation is given by the orientation of the surface normal of this plane, which is expressed either by the normalized vector $\vec{n}$ or by the two angles (φ, ψ):

$$\varphi = tan^{-1}\frac{\sqrt{a^2 + b^2}}{c}$$

$$\psi = tan^{-1}\frac{b}{a}$$

4. Performance of the Proximity Sensor

The performance of the prototype proximity sensor was tested for a surface at various distances and orientations. The test surface was a planar piece of white cardboard. This test plane is placed on a precision positioning table with an angular motion (resolution of 1 arc minute) and a linear motion (resolution of 0.00254 mm). The test surface is moved from the near limit of operation (41mm) to the far limit (51mm) with increment of 0.5 mm, and rotated from $+30^{\circ}$ to -30° with increment of 2°. The rotation was about the y axis; that is, the surface normal vector stays on x-z plane. Four complete sets of data, each of which covers all the combinations of distance and orientation, were taken. The results shown in this section are the averages over these sets. All the testing is done in a dark environment to eliminate extraneous light.

The performance was evaluated by examining the following: The first measure is a chip spot trajectory that the intensity center of the spot takes across the sensor chip face as the surface is moved and rotated in front of the sensor. The second measure is the ability to accurately locate spots for each LED in three-dimensional space. The third measure is the ability to accurately determine the distance and orientation of the plane in three-dimensional space. This last measure is most indicative of overall system performance.

To make the proximity sensor operational requires calibration. At known positions of the surface, the center positions of the light spots on the surface were located by using an infrared scope. This was done only for 10 positions of the plane in the orientation perpendicular to the optical axis. For these spot positions we

took the readings of the sensor outputs. From this data, we determined the system constants used in triangulation such as line trajectories of light beams and the coefficients of the error polynomials.

Chip Spot Trajectory

Figure 9 shows the chip-spot trajectories for a plane orthogonal to the optical axis moved various distances without rotation. We moved the test plane from the near limit of operation. From the optical geometry, we expect to obtain straight lines of trajectories which are 60^{o} apart. The figure has essentially this behavior, though the light sources are not completely aligned. For each trajectory the chip spot moves towards the center of the sensor chip as the plane approaches the point where the light source beam approaches the optical axis (d). The ends of the trajectories bend due to nonlinearity of the sensor chip.

Chip-spot trajectories are also measured when the test plane is placed at a fixed distance and is rotated from $+30^{o}$ to -30^{o}. The result is shown in Figure 10, which shows the behavior we expect.

Location of Spatial Points

The error in locating spatial points is defined as the difference between the actual spatial position and the measured spatial position. The actual spatial position is the position at which the light source trajectory intercepts the test plane. The measured spatial position is obtained by performing triangulation with the error correction.

Quantitative data concerning the error in locating spatial points is shown in Table 1. The averages and standard deviations of errors in x, y, and z are shown for various plane rotation angles. The average is taken over all the LEDs and distances. We can see that the errors are very small (order of .01 mm) when the plane is nearly perpendicular to the optical axis, and that they increase as the plane is rotated further from being orthogonal to the optical axis. This is because the intensity center shifts from the idealized line trajectory of light source beam. Of course we must note that in some extreme cases the spots are out of sight from the sensor chip. In the normal operational range, the error is in order of 0.1 mm. The average error in the distance (z) for a particular LED (no. 2) is shown in Figure 11, which shows dependency of the error on the distance and the angle.

Distance and Orientation of Planes

By fitting a plane to the six spatial points we determine the plane equation (10) above. The discrepancy of this plane from the actual plane which is derived by the known position and angle of the test surface can be characterized by two quantities: the error in distance evaluated by the difference of the D values defined by (11) above for the two planes, and the error in orientation evaluated by the angle made by the surface normals

of the two planes.

The two types of error in determining planes are displayed in Figure 12 (location error) and in Figure 13 (orientation error): the average error is plotted as a function of actual distance and orientation. Table 2 quantifies the error by listing the averages and standard deviations vs. various actual plane angles. From this data, we can see the following. First, Figures 12 and 13 show that there is a large circular region of distance and orientation for which the sensor operates with accuracy. Within this region, the error is typically less than 0.07mm in distance and 1.5° in orientation. Second, the error in determining the plane is substantially reduced from that of an individual point. The redundancy in measurements (using six points for plane fitting) results in this improvement. Third, the error plots in Figures 12 and 13 has a small ridge along the distance of 45 mm. This is due to the fact that the plane fitting actually has a singularity near the tip of the light beam cone because all the measured spatial points come very close. In the prototype, the light sources are not completely aligned and the singularity did not show up too conspicuously.

5. Conclusion

We have presented the theory, implementation, and performance of an optical proximity sensor capable of measuring locations and orientations of local surface patches. This sensor has a precision of 0.07mm and 1.5° over the range of 40mm to 50 mm and $+30^{\circ}$ to -30°. It can generate up to 1000 measurements per second. The features of the sensor include simplicity in principle, fast speed, and precision by exploiting the geometrical redundancy. The concept can be easily extended to various other configurations which are suited for individual applications. Currently we are building a new version of the sensor by improving the following points:

- Use of modulation for operation under ambient light
- Use of fiber cables and laser diodes for better light sources
- Use of double cones for eliminating the singularity of plane fitting

Acknowledgements

We thank Michael Fuhrman for useful discussions, and Regis Hoffman and Ed Kurtz for help in software and hardware development.

References

[1] Johnston, A. R.
Optical Proximity Sensing for Manipulators.
Technical Report JPL TM 33-612, Jet Propulsion laboratory, 1973.

[2] Kanade, T., Asada, H.
Noncontact Visual 3-D Sensing Devices.
In *SPIE Technical Symposium East '81, 3-D Machin Perception (Vol. 283).* Society of Photo-Optical Instrumentation Engineers, 1981.

[3] Okada, T.
Development of an Optical Distance Sensor for Robots.
Robotics Research 1(4):pp. 3-14, 1982.

Table 1: Table of the averages and standard deviations of error in locating spatial points.

plane angle (degrees)	X error (millimeters)		Y error (millimeters)		Z error (millimeters)	
	e_x	σ_e	e_y	σ_e	e_z	σ_e
+30	.0485	.1812	.0301	.1772	-.0981	.2025
+20	.0231	.1224	.0265	.1175	-.0470	.1340
+10	-.0073	.0662	.0024	.0489	-.0250	.0766
0	-.0024	.0202	.0016	.0187	.0056	.0136
-10	-.0475	.1434	.0608	.1502	.1133	.1247
-20	-.1227	.2742	.1173	.3038	.2373	.2669
-30	-.1177	.2958	-.0837	.5246	.4511	.5756

Table 2: Table of averages and standard deviations of error in determining planes.

plane angle (degrees)	plane orientation error (degrees)		plane distance error (millimeters)	
	e_θ	σ_e	e_D	σ_e
+30	4.9277	.6941	-.1400	.0165
+20	1.9743	.7346	-.0832	.0206
+10	1.4195	.5896	-.0346	.0174
0	.5314	.2801	.0106	.0102
-10	1.0607	.4036	.0635	.0168
-20	3.7676	3.3802	.1365	.0602
-30	3.1996	1.1282	.1816	.0115

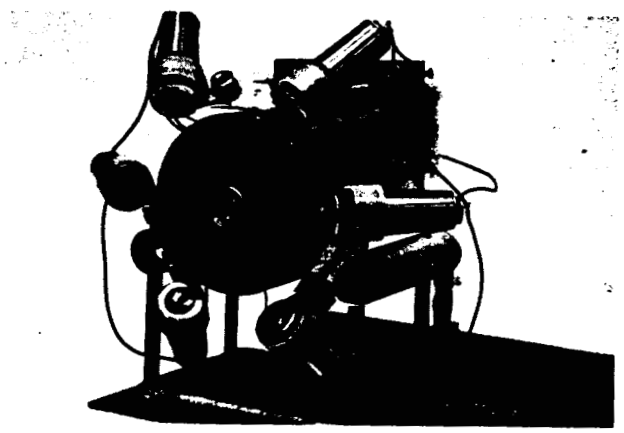

Figure 1: Photo of the prototype proximity sensor; 8cm (diameter) × 10cm (length).

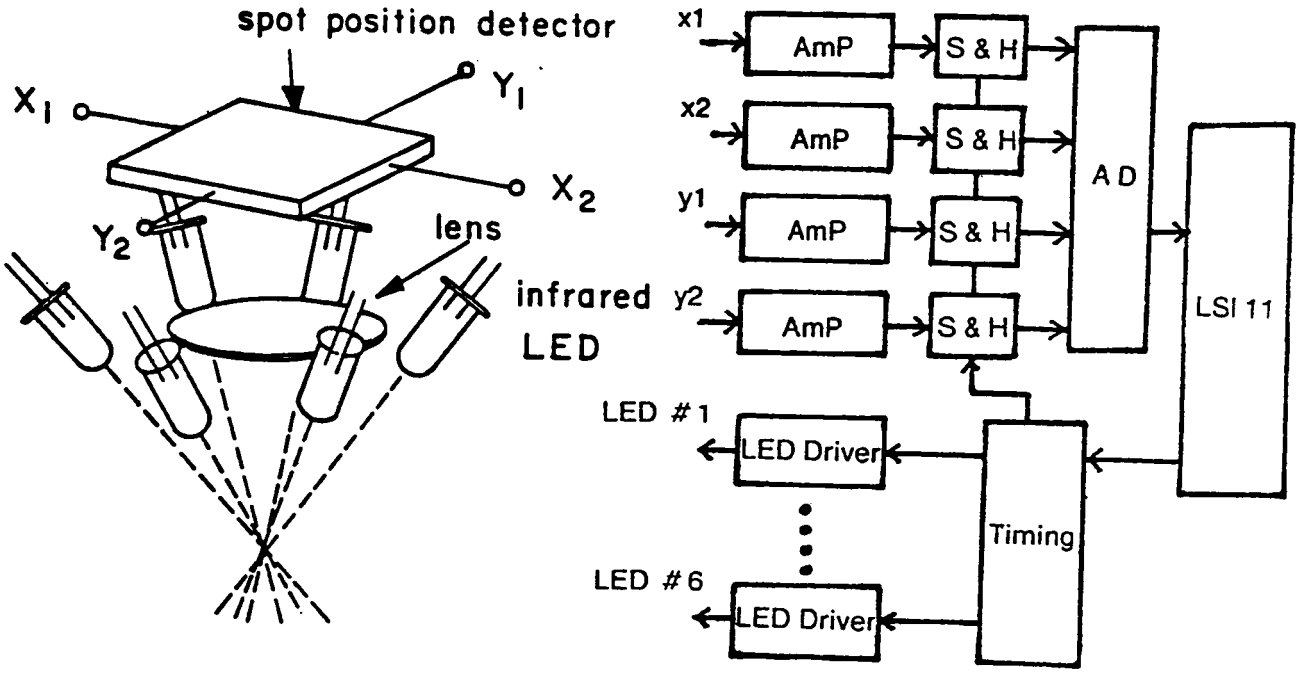

Figure 2: Configuration of the proximity sensor.

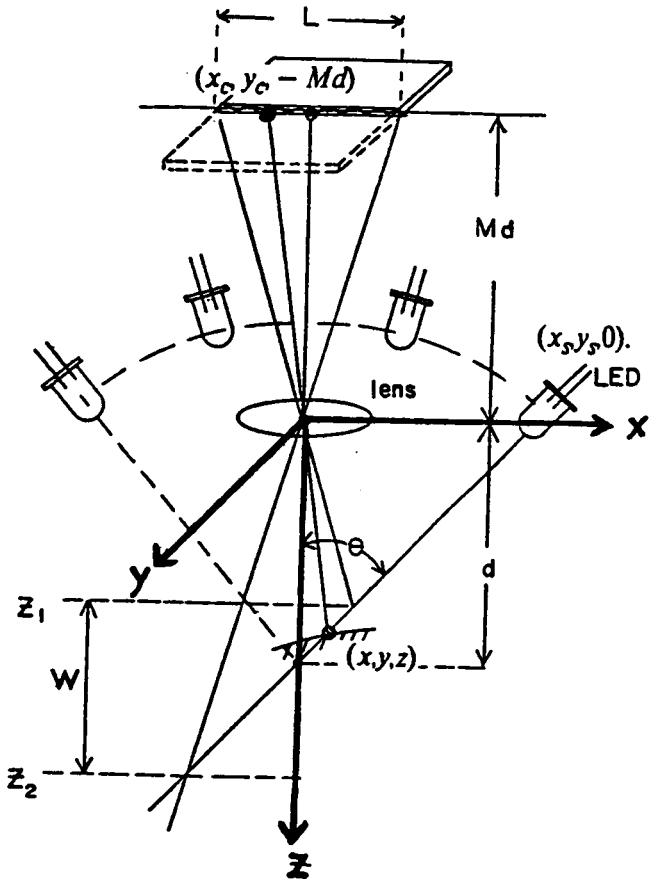

Figure 3: The geometry for distance measurement.

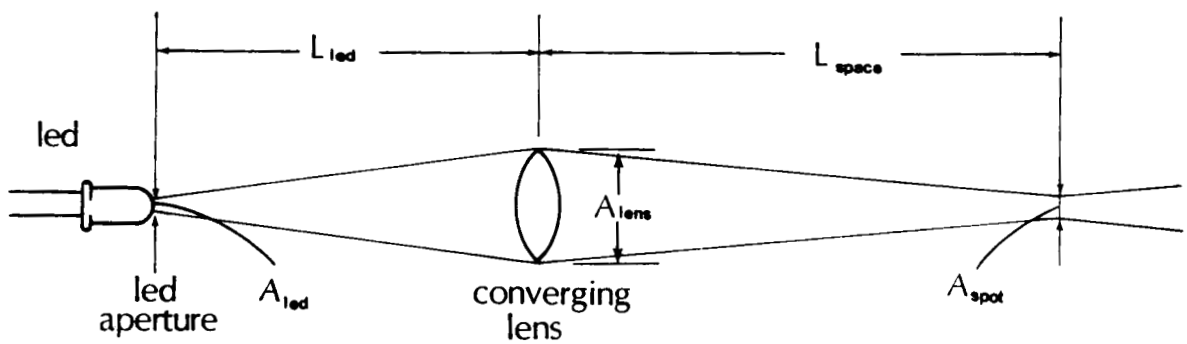

Figure 4: Configuration of light source. With $d = 45$ mm and $\theta = 45^{\circ}$, the distance l_{space} of the best focus is designed to be $d/cos\theta = 63.6$ mm.

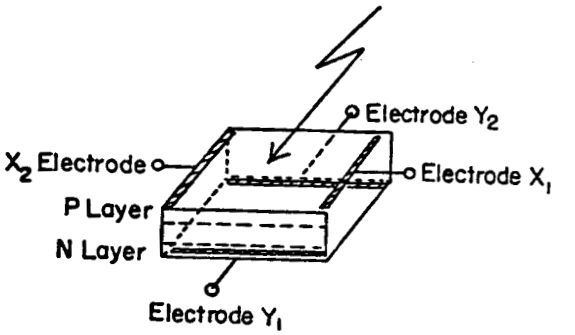

(a)

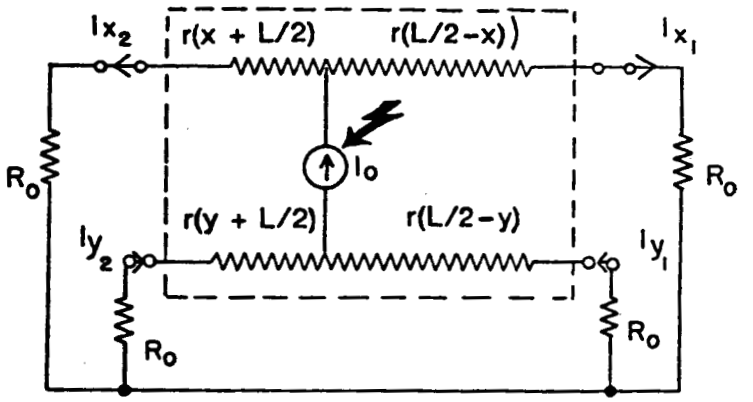

(b)

Figure 5: Functional diagram of the sensor chip.

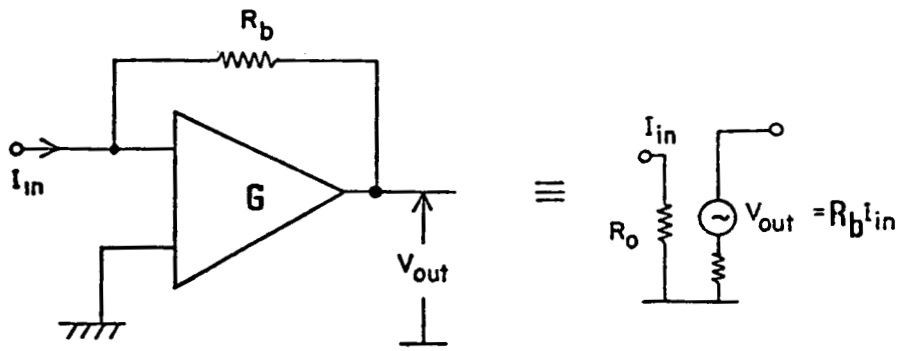

Figure 6: Current-to-voltage converter

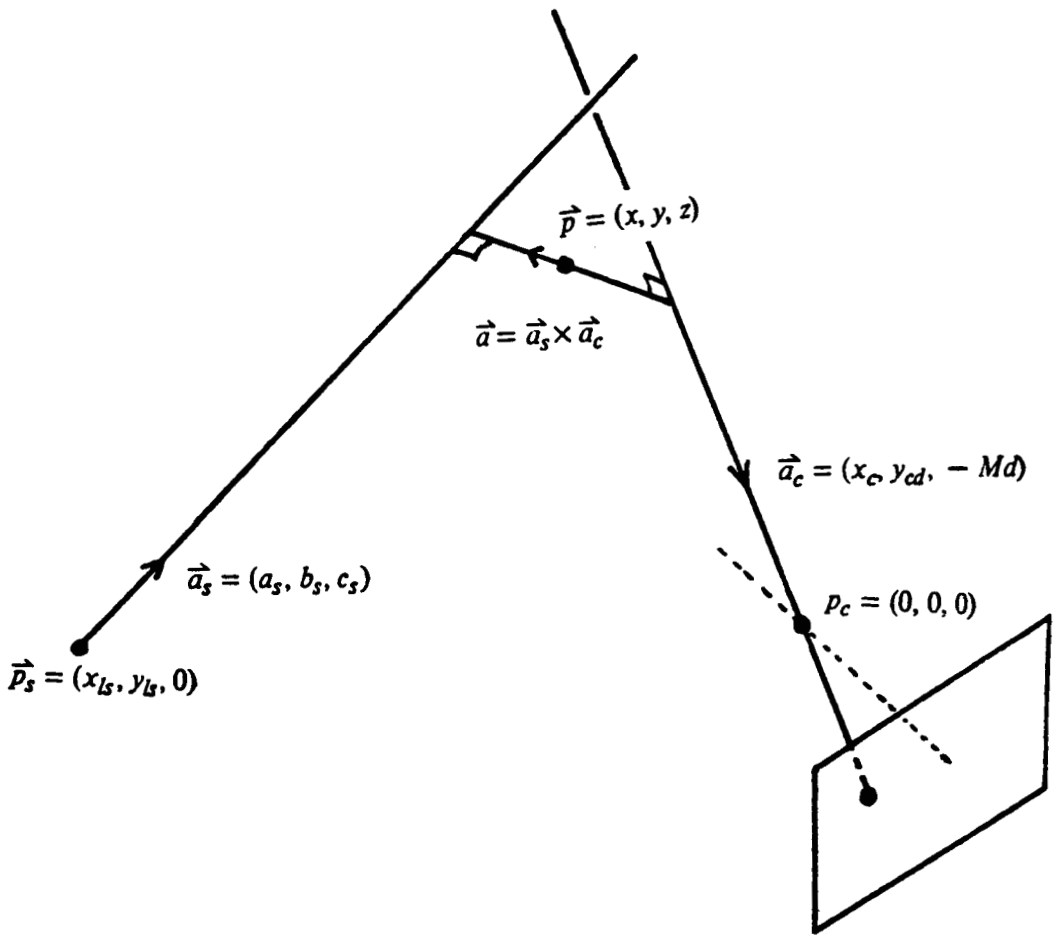

Figure 7: Locating a spatial point on the line of shortest distance between two lines.

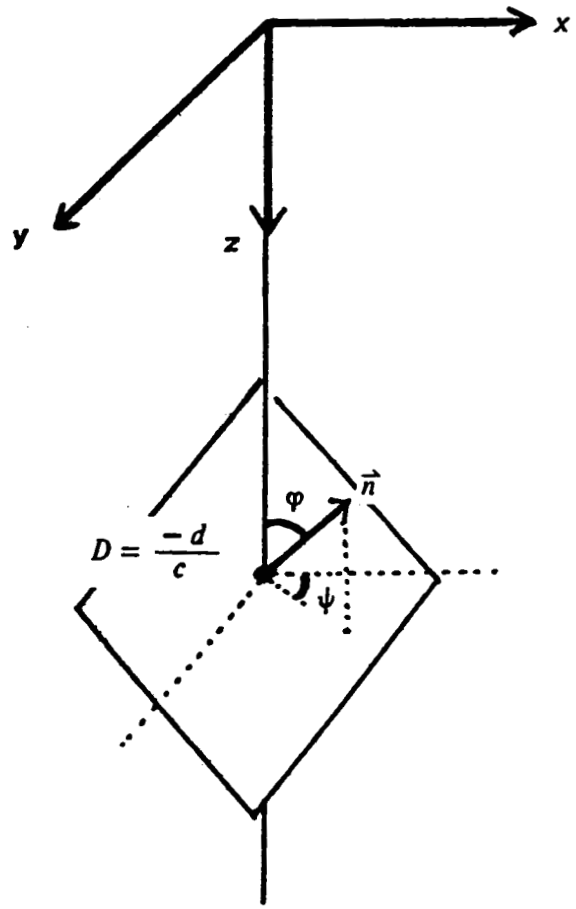

Figure 8: Defining the distance and orientation of a plane.

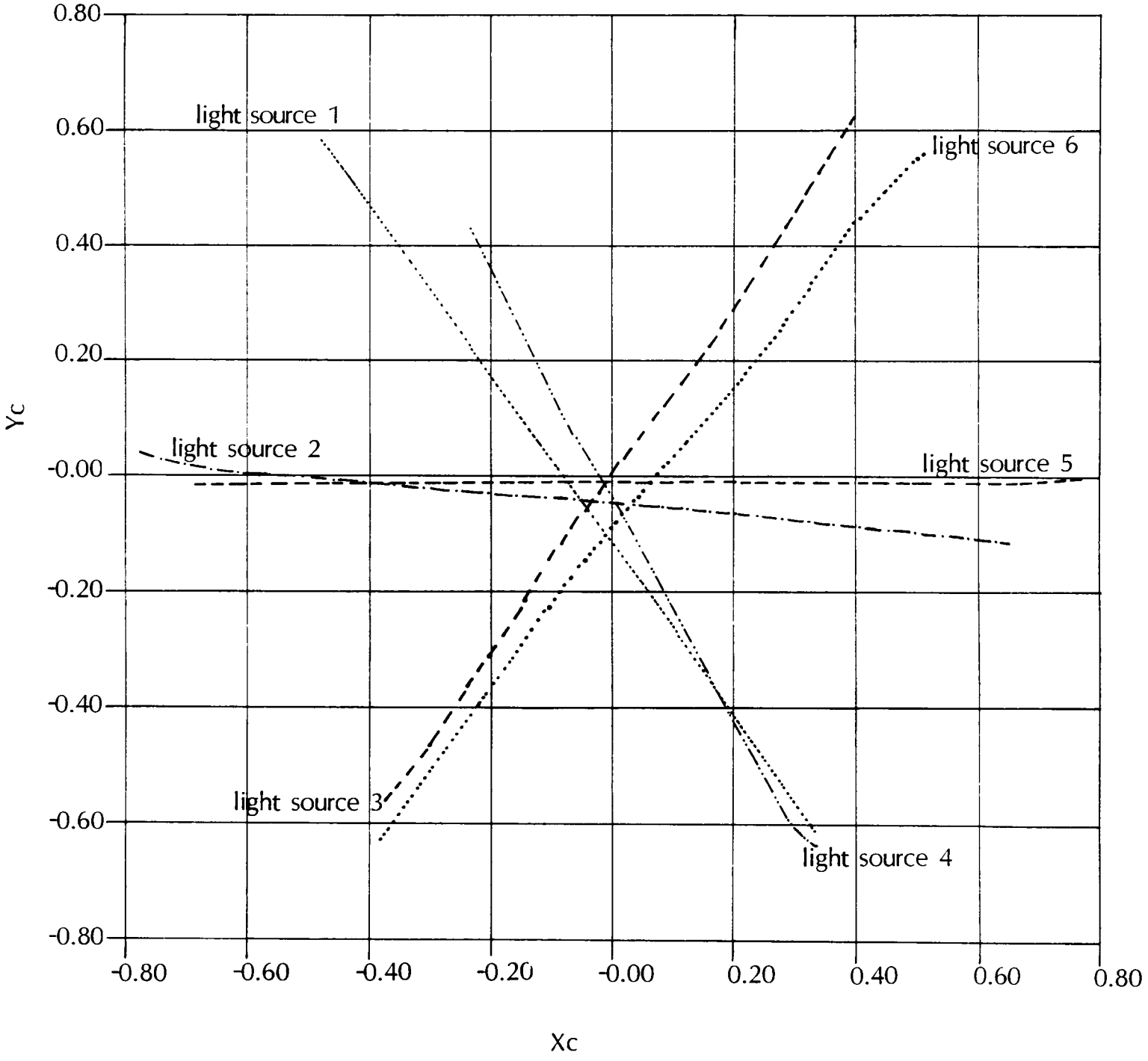

Figure 9: Chip-spot trajectories for a perpendicular plane.

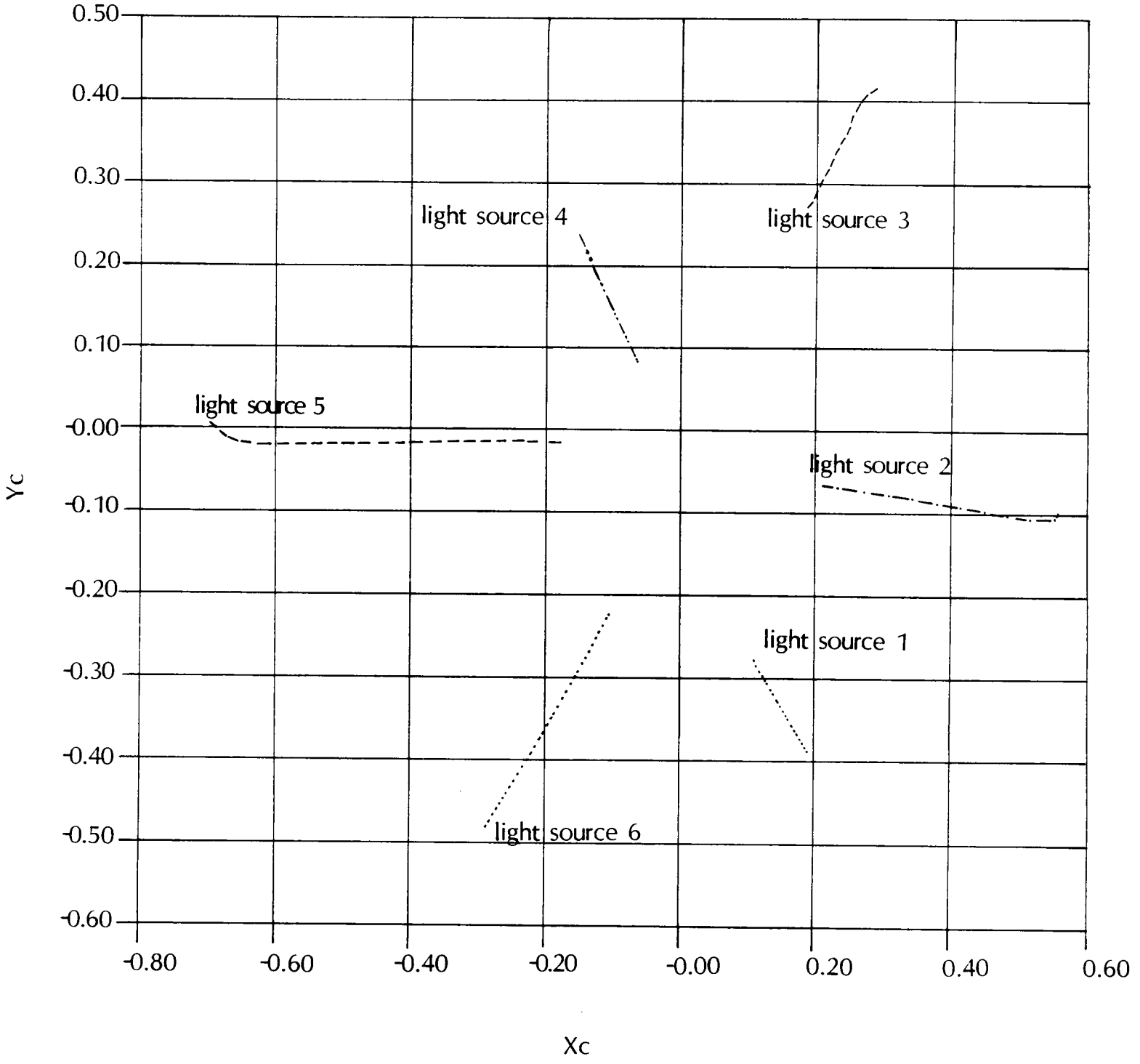

Figure 10: Chip-spot trajectories for a rotating plane.

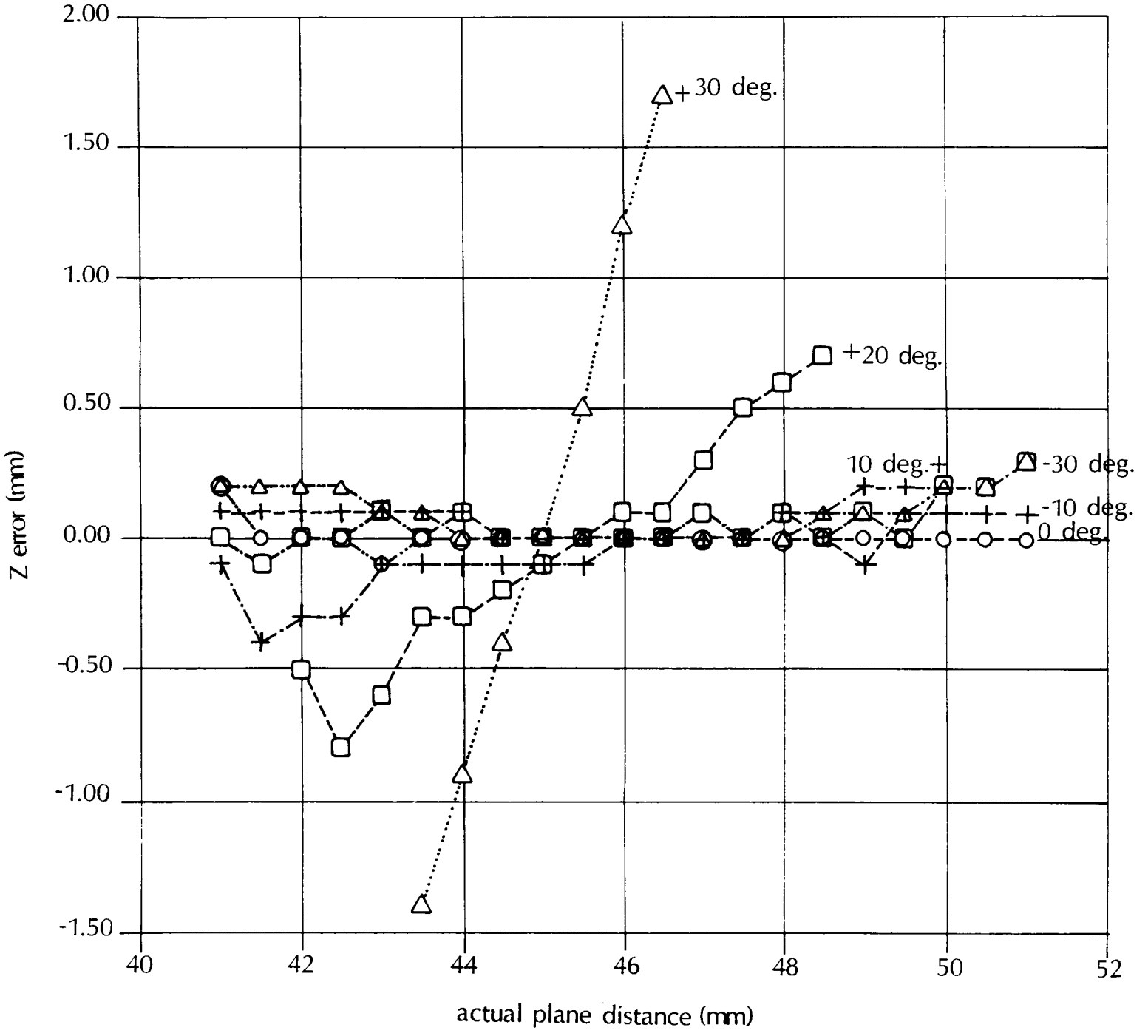

Figure 11: The average error in the distance (z) for a particular LED (no. 2)

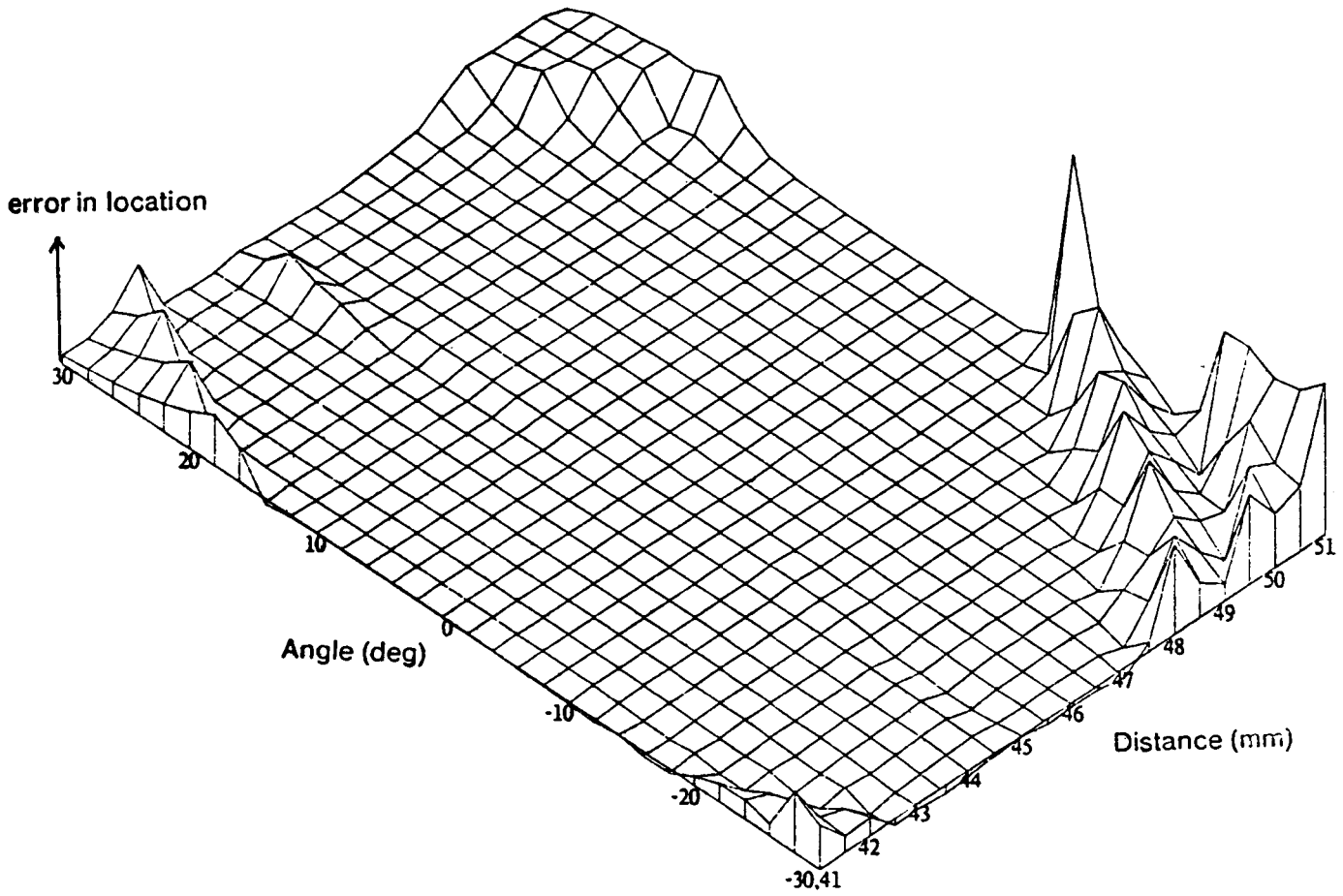

Figure 12: Plot of error in the distance of plane.

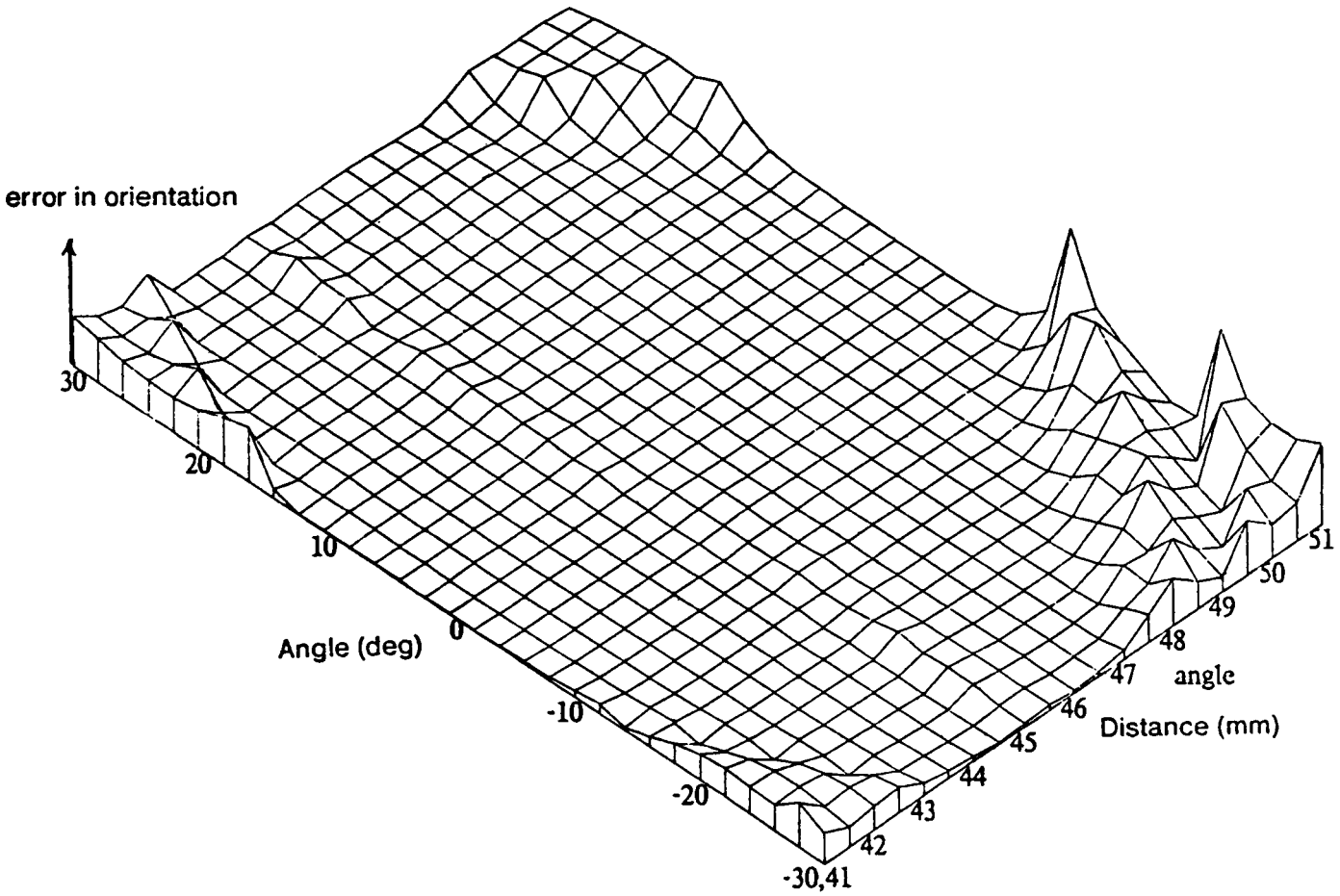

Figure 13: Plot of error in the orientation of plane.

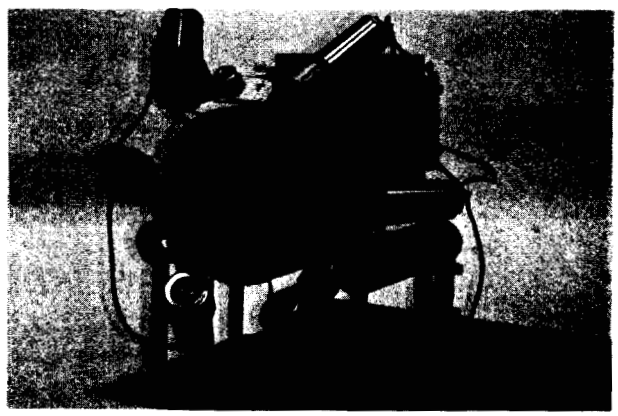

Figure 1: Photo of the prototype proximity sensor; 8cm (diameter) × 10cm (length).

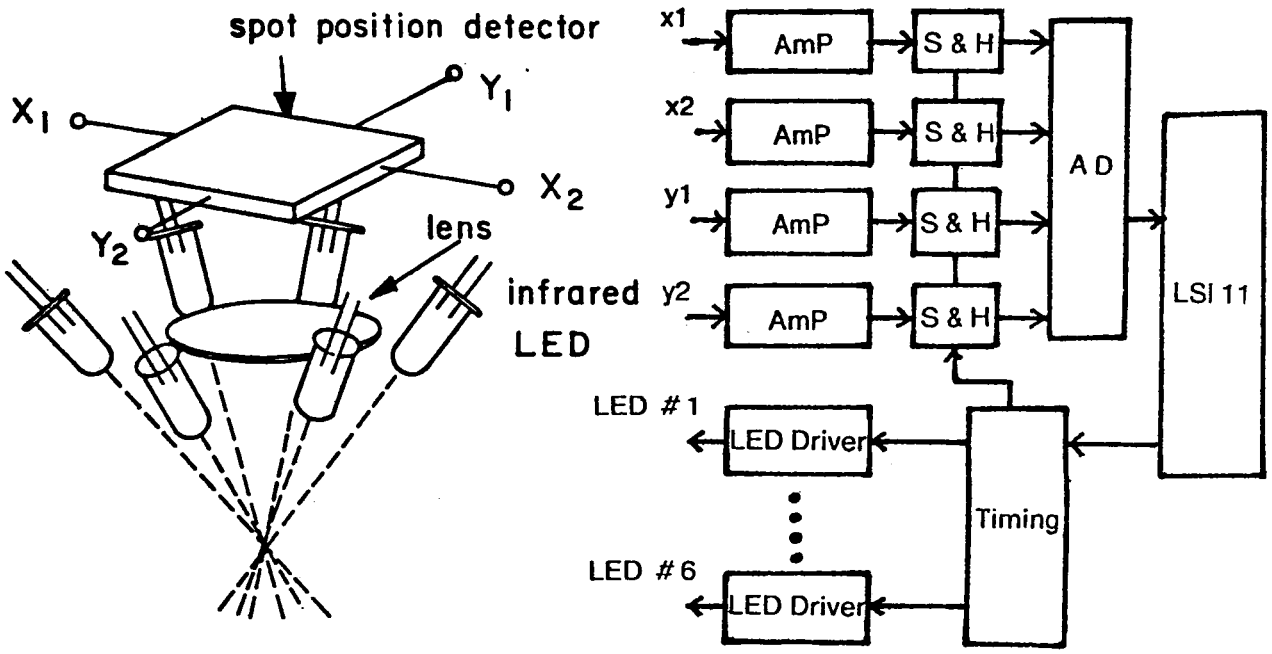

Figure 2: Configuration of the proximity sensor.

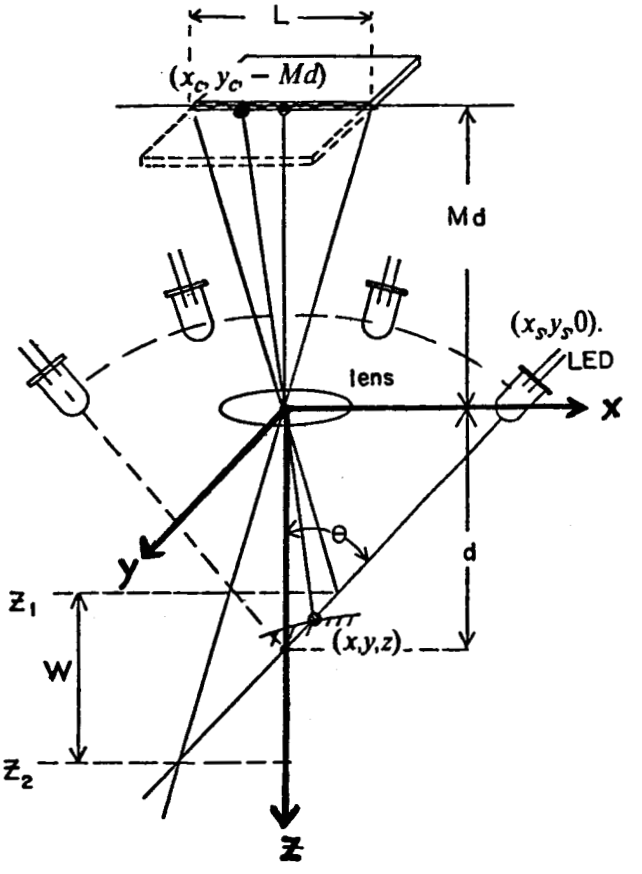

Figure 3: The geometry for distance measurement.

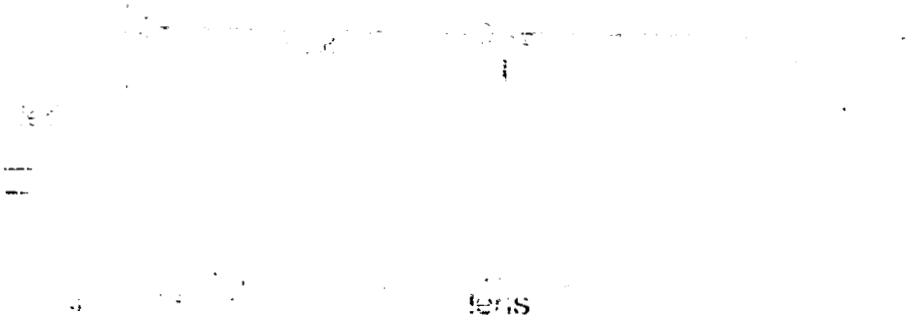

Figure 4: Configuration of light source. With $d = 45$ mm and $\theta = 45^{\circ}$, the distance l_{space} of the best focus is designed to be $d/cos\theta = 63.6$ mm.

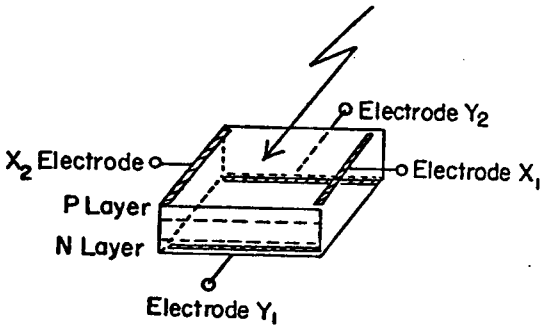

(a)

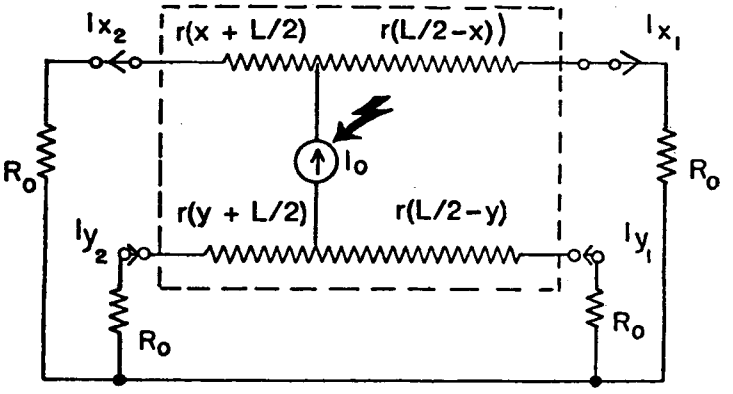

(b)

Figure 5: Functional diagram of the sensor chip.

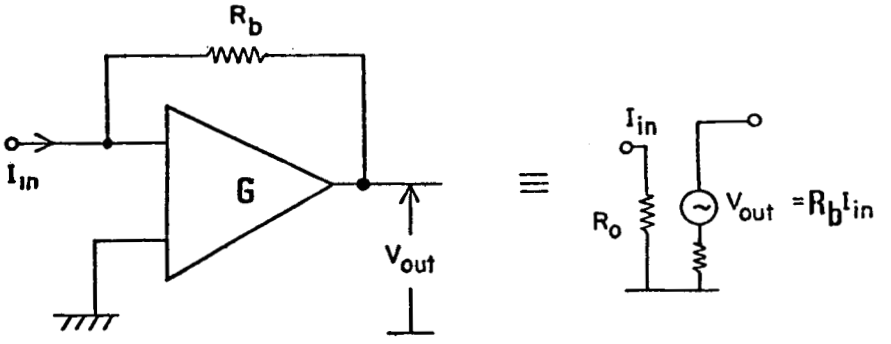

Figure 6: Current-to-voltage converter

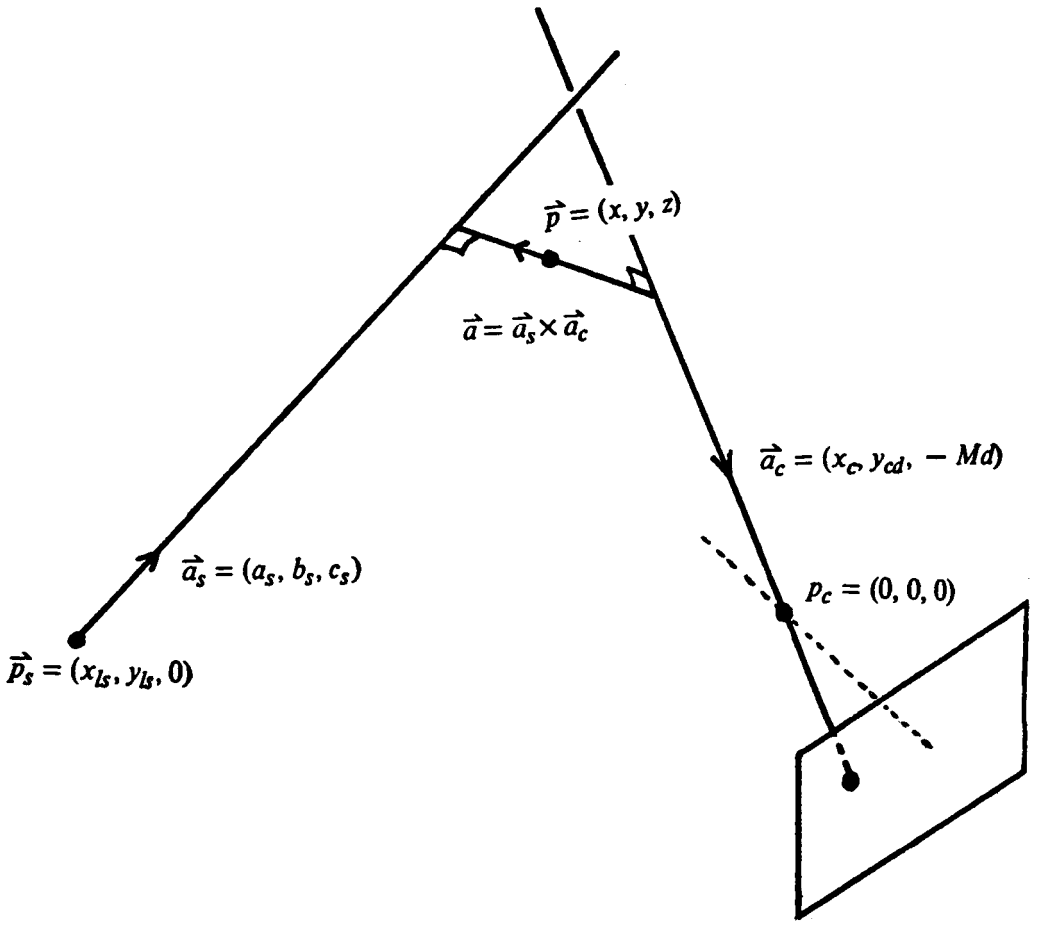

Figure 7: Locating a spatial point on the line of shortest distance between two lines.

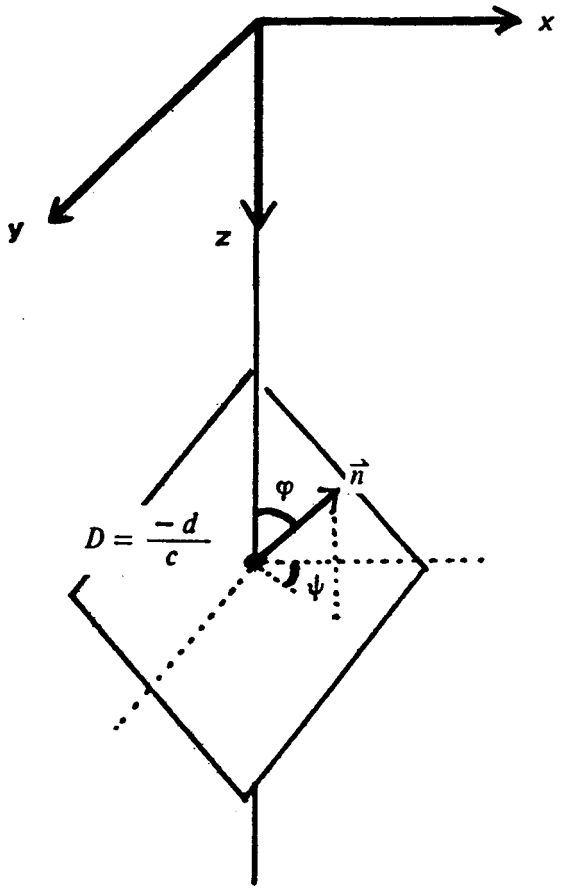

Figure 8: Defining the distance and orientation of a plane.

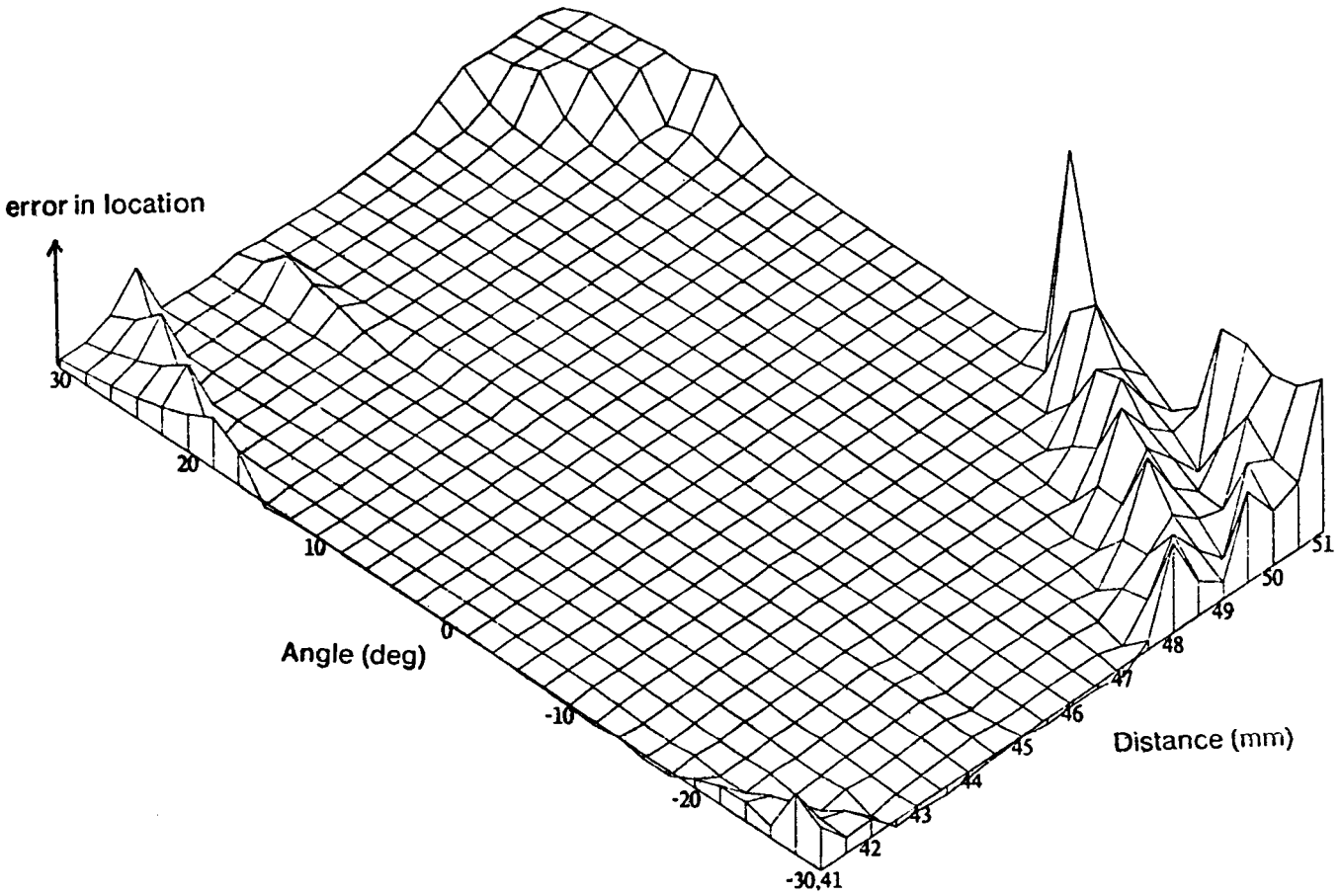

Figure 12: Plot of error in the distance of plane.

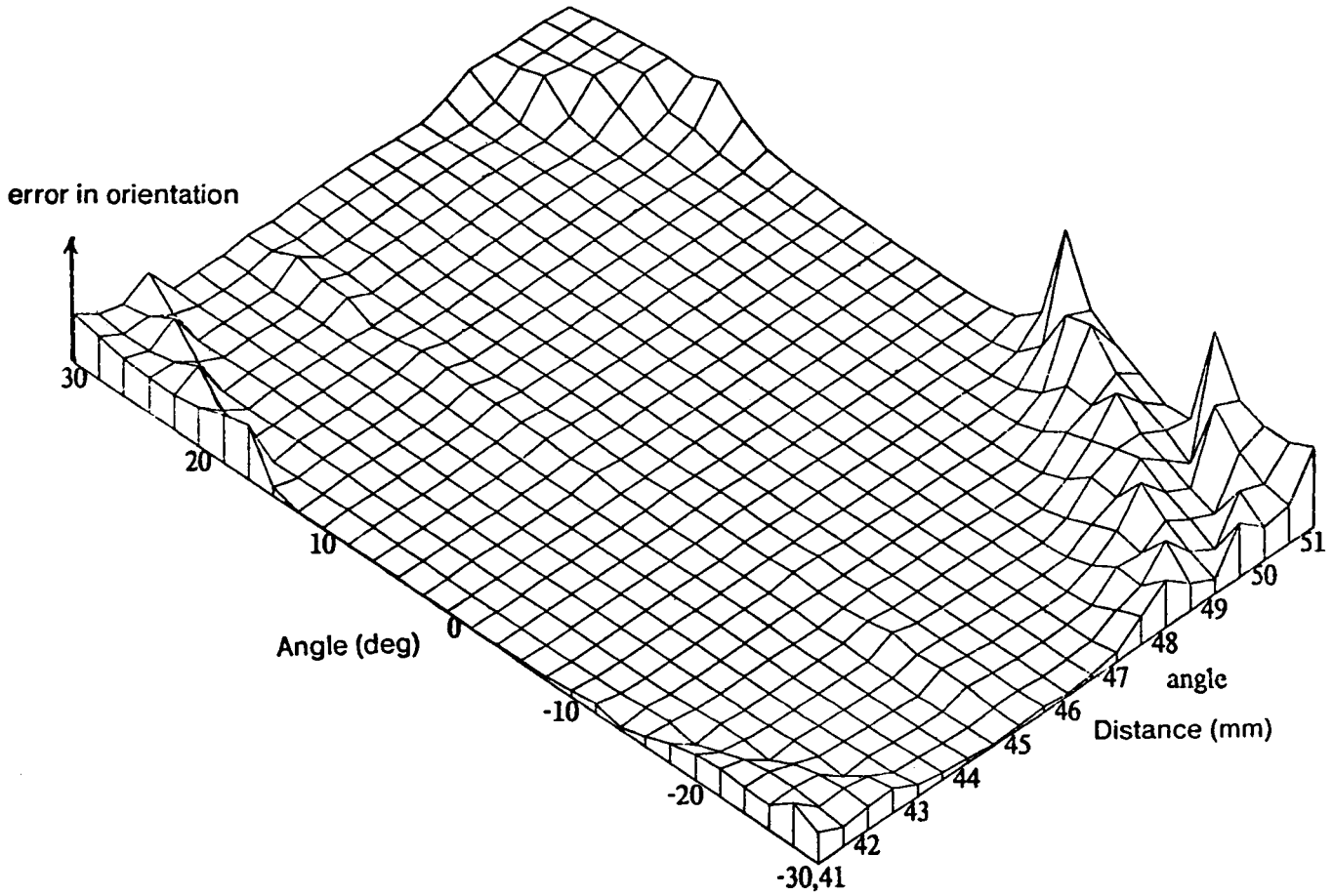

Figure 13: Plot of error in the orientation of plane.